

# Two typical collective behaviors of the heavy ions expanding in cold plasma with ambient magnetic field

Guo-Liang Peng

*Beijing Institute of Technology, Beijing 100081, China and  
Northwest Institute of Nuclear Technology, Xi'an 710024, China*

Jun-Jie Zhang, Jian-Nan Chen, Tai-Jiao Du, and Hai-Yan Xie

*Northwest Institute of Nuclear Technology, Xi'an 710024, China*

(Dated: April 9, 2021)

We have numerically studied the evolution of the heavy ions that expand in a cold background plasma at a large scale. Two typical collective behaviors of the heavy ions are identified with the conditions where only the traversing heavy ion's initial total mass is different. Our work has demonstrated that a difference in the initial total mass of the moving heavy ions is able to induce completely different collective behaviors of the plasma. The simulation is performed via the hybrid model, in which the ions and electrons are treated as classical particles and mass-less fluid, respectively. Due to the imbalance of the electric and magnetic force on the heavy ions, these particles will evolve into different collective patterns at the later time. These patterns manifest a rather different stopping behavior of the moving ions and an opposite drifting direction of the electron fluid at the rim of the expanding plasma. Further numerical and analytical calculations show that the imbalance depends not only on the number densities of the plasma ions, but also on the spatial variations of the magnetic fields. Our work reveals that the collective behavior of the heavy ions is highly non-linear, and the non-linearity is able to induce different phenomena in the evolution of the system at a large scale.

## I. INTRODUCTION

When a patch of heavy ions expands and traverses a magnetized background plasma with a high velocity, a super-Alfvénic shock will be formed at the front of the moving ions[1, 2]. In such a condition, the heavy ions disturb the background plasma and may form a magnetic cavity[3] at a large scale. Our present work has identified two typical collective behaviors of the heavy ions expanding in a dilute cold background plasma with the existence of an ambient magnetic field. These conditions have many practical and potential correspondences, such as the solar wind in near space environment[4–6], planetary atmospheric plasma[7–10] and other similar effects[11–15].

In these conditions, the mean-free-path of the expanding heavy ions usually takes a few hundred kilometers. As the ions (e.g. iron ions) expand in the dilute background plasma, collisionless shocks[16, 17] will appear and influence the later collective behavior of these ions. Along with the ion-evolution, a flute mode (caused by the flute instability[18]) may be generated before they finally stop moving[18, 19].

Due to the non-linearity of the plasma and the limited experimental data at such a large scale (a few hundred kilometers), various phenomena of this kind of physical process remains to be investigated. This paper focuses on the stopping behavior and mass influence of the heavy ions. The simulation is performed via the hybrid model[1, 20–25], which treats the ions as PIC (Particle-In-Cell) particles and the electrons as mass-less fluid to neutralize the plasma. To understand how the initial mass of the heavy ions influences their subsequent behavior, we have chosen two typical conditions where only the initial mass of the heavy ions is different. These two conditions correspond to the atmospheric phenomena in near space[4–6, 26] ( $\Gamma \ll 1$ , expression of  $\Gamma$  is in Eq. (7)) and the laser experiments ( $\Gamma \geq 1$ )[14, 27–32].

Our studies find that if the total mass of the heavy ions are small, they rotate in the ambient geomagnetic field and couple weakly with the background plasma (Fig. 3), which corresponds to the decoupled phenomena in Ref. [1]. The collective rotation of these ions produces a breathing pattern (Fig. 2 and 4) which is quite different from the  $\Gamma \ll 1$  simulation (Fig. 1), where the ions expand nearly in a straight line and curve at the end without a breathing pattern (Fig. 5). To analyze the possible mechanism for the breathing pattern, we have chosen four heavy particles, and depicted their electric and magnetic forces (Fig. 3 and 5). From the analysis of the forces, we find that the imbalance of the electric and magnetic forces in the  $\theta$  direction is the main contributor to the breathing pattern and the flute mode (Eq. (12)). Moreover, the directions of the electron drift are also different at the rim of the expanding torus in the two cases (Fig. 6). The difference of the electron drift can affect the stopping behavior of the ions (Fig. 7).

The paper is organized in the following structure. In section II, we have briefly introduced the theoretical set-up of the hybrid model and performed a  $\Gamma \ll 1$  simulation. In section III, we have presented the simulation results of the breathing pattern and depicted the relevant forces and motion of the debris ions. The conclusion is made in section IV.

## II. THE SIMULATION MODEL

When the gyro-radii of the heavy ions are about a few hundred kilometers which are comparable to the ion mean-free-path, the Knudsen number is larger than one and the kinetic effect plays a more important role than the fluid effect[26]. In this condition, MHD (Magneto-Hydro Dynamics) calculations cannot be trusted. In this work we use the so called hybrid plasma simulation model to perform the particle evolution and analyze the collective motion of the heavy ions.

The hybrid model starts with the equation of motion for electrons. In S.I. unit this reads[1]

$$m_e n_e \frac{d\mathbf{u}_e}{dt} = \nabla(n_e k T_e) + en_e(\mathbf{E} + \mathbf{u}_e \times \mathbf{B}) - en_e \eta (\mathbf{J}_i + \mathbf{J}_e), \quad (1)$$

where  $m_e$ ,  $n_e$ ,  $\mathbf{u}_e$ ,  $T_e$  and  $\mathbf{J}_e$  are the mass, number density, fluid velocity, temperature and electric current for electrons, receptively. Vectors  $\mathbf{E}$  and  $\mathbf{B}$  denote the electric and magnetic field acted upon the electrons. Constants  $e$ ,  $k$  and  $\eta$  are the electronic charge, the Boltzmann constant and the electric resistivity.  $\mathbf{J}_i$  represents the ion electric current.

Currently we mainly focus on the conditions where the typical electron gyro-radius and Debye length are about a few to a hundred centimeters. In these conditions, the detailed motion of the electrons are negligible compared to that of the ions. Thus, it is reasonably acceptable to assume that: i) all electrons are mass-less and ii) the electric field applied on the electrons are so strong that the electrons respond instantly to the electric field and always neutralize the ions[22]. These assumptions reduce the computational cost needed for tracking the information of electrons. For mass-less electrons, the left hand side of Eq. (1) equals zero. For numerical convenience, we may further assume that the gradient of the electron temperature and the electric resistivity are small[1], hence, we can explicitly express  $\mathbf{E}$  from Eq. (1) as,

$$\mathbf{E} = -\mathbf{u}_e \times \mathbf{B}. \quad (2)$$

Since we focus on the ion-motion in large spatial and time scales, the propagation of high-frequency radiations is not of much interest. This allows us to drop the displacement current in Maxwell's equations and simply adopt the Ampere's law for the electron fluid velocity  $\mathbf{u}_e$ ,

$$\begin{aligned} \nabla \times \mathbf{B} &= \mu_0 \left( \sum_{\text{ion-species}} \mathbf{J}_i + \mathbf{J}_e \right) \\ &= \mu_0 \left( \sum_{\text{ion-species}} \mathbf{J}_i - en_e \mathbf{u}_e \right), \end{aligned} \quad (3)$$

where  $\mu_0$  is the vacuum permeability. Note that Eq. (3) is a rather stronger approximation than the usual Darwin limit[22, 33]. In Darwin limit only the solenoid part of the displacement current is neglected. This means that in our calculation both  $\mathbf{B}$  and  $\mathbf{E}$  reach the asymptotic limit at each time step. Combining Eq. (2) and (3), we can write the electric field  $\mathbf{E}$  in terms of magnetic field  $\mathbf{B}$  and ion current  $\sum_{\text{ion-species}} \mathbf{J}_i$ ,

$$\mathbf{E} = -\frac{1}{en_e} \left( \sum_{\text{ion-species}} \mathbf{J}_i - \frac{\nabla \times \mathbf{B}}{\mu_0} \right) \times \mathbf{B}. \quad (4)$$

Finally we use

$$\nabla \times \mathbf{E} = -\frac{\partial \mathbf{B}}{\partial t} \quad (5)$$

and

$$n_e = \sum_{\text{ion-species}} (Z_i n_i) \quad (6)$$

to close Eq. (4), where  $Z_i$  and  $n_i$  denote the charge state and number density of the ions, respectively. In Eq. (6) we have used the above mentioned neutrality assumption.

To solve Eqs. (4) ~ (6), the finite difference method is utilized with all ions treated as PIC particles. Given the initial distribution of the background plasma and the rapidly moving heavy ions in phase space, the evolution of all ions in the ambient magnetic field can be obtained accordingly.

For an physical intuition of the ions evolution, we have performed a 3D simulation in which a patch of heavy ions expanding in the cold plasma with the presence of ambient geomagnetic field (see Fig. 1). The background particles are taken to be the Oxygen ions which are distributed uniformly in spatial grids with a constant number density. The heavy ions are Iron ions which initially locate at the point (0, 0, 0). The heavy ions traverse the background plasma at a constant initial velocity and evolve into a thin shell with flute modes at some later time.

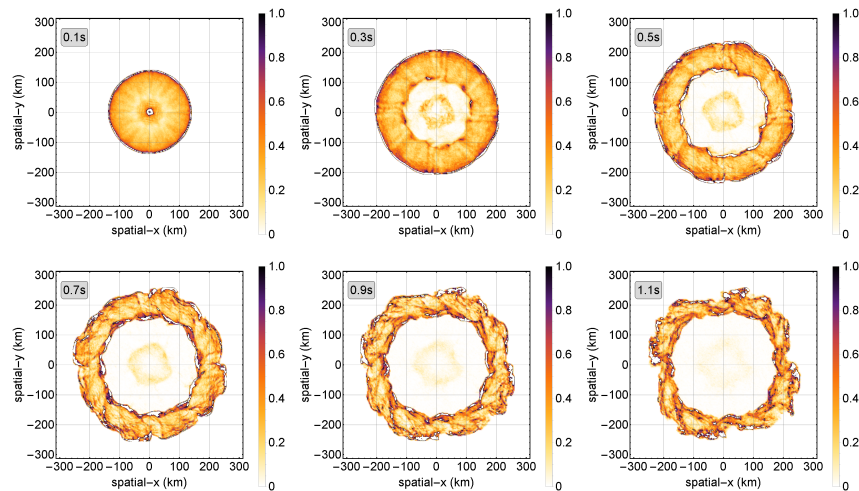


FIG. 1: Evolution of the heavy ions at various snapshots with  $\Gamma \simeq 0.03$ . The figures are viewed in the direction of the ambient magnetic field, which points out of the plane with initial value  $\mathbf{B}_0 = 0.5 \times 10^{-4}$  T throughout the spatial grids. The heavy ions are Iron particles with charge state  $Z_{i,\text{Fe}} = +1$ . All heavy ions are initially placed at spatial point  $(0, 0, 0)$  with radial velocity  $v_{i,\text{Fe}} = 2 \times 10^6$  m/s.  $10^3$  kg heavy ions are used in total. The number density of the background ions (Oxygen) are taken to be  $10^7$  /cm<sup>3</sup> with charge state  $Z_{i,\text{O}} = +1$ . One sees clearly that the flute mode occurs at some later time steps.

The flute mode is a typical phenomenon in this condition. To measure its occurrence, the usual parameter used is the ratio[29]

$$\Gamma = \rho_i / R_3, \quad (7)$$

where  $\rho_i$  is the direct ion gyro-radius and  $R_3$  is the magnetic confinement radius.  $R_3$  can be obtained by equating the initial kinetic energy of the heavy ions with the equivalent magnetic field energy in a volume of radius  $R_3$ ,

$$E_i = \frac{1}{2} \frac{\mathbf{B}^2}{\mu_0} \frac{4}{3} \pi R_3^3, \quad (8)$$

where  $E_i$  is the total initial kinetic energy of the heavy ions. When  $\Gamma \gtrsim 1$ , like in laser or space experiments [27–32], the flute mode will be less clear. When  $\Gamma \ll 1$ , a strong flute mode will occur.

One also sees the reflected ions in the middle of the torus at  $t = 0.3$  s in Fig. 1. Due to the finite computing region, these reflected ions gradually run out of the computing domain and eventually fade away. The reflected ions play an important role in the formation of the shock structure and influence the stability of the plasma[16, 34, 35].

### III. TWO TYPICAL PATTERNS OF THE HEAVY IONS

The two typical patterns of the heavy ions can be determined by their initial total mass. The difference in the total mass will lead to different  $\Gamma$  values defined in Sec. II. We will demonstrate the simulation results of two values  $\Gamma = 1.09$  (Fig. 2 and 4) and  $\Gamma = 0.03$  (Fig. 1) which correspond to the laser experiments and the near space plasma.

Fig. 2 gives the evolution of the heavy ions when  $\Gamma \simeq 1.09$ . In such a condition like in the laser experiments, we see a very different pattern of the ion-motion compared with that in Fig. 1. The heavy ions initially expand outward and begin to form a thin shell. Quite unexpectedly, these ions then stop expanding and shrink back into the burst point. This breathing pattern continues until most of the ions lose their energy to the background plasma and finally stop moving.

To see exactly what happens to these ions, we have picked four ion particles and tracked their motions at each snapshot. As is depicted in Fig. 3, the Lorentz force is always perpendicular to the motion of the particles. However, the electric force, which is initially perpendicular to the trajectories of the particles, gradually tilts parallel to the velocity of the heavy ions at the rim of the thin shell. The parallel electric force is the main contributor that decreases the energy of the heavy ions and meanwhile generates a circular electric field that propagates outward.

One may suspect that this breathing pattern is caused by the initial set-up of constant radial velocity since the collective motion of these ions is sensitive to their initial velocity. In fact, the breathing pattern is mainly determined by the initial mass of the heavy ions and is not so sensitive to the initial distribution of their velocities. To perceive this argument, we have demonstrated a case in which the ions initial velocities are sampled from a Maxwellian distribution, as in Fig. 4. We see clearly that the breathing pattern still dominates the evolution of the heavy ions except for an absence of a thin shell.

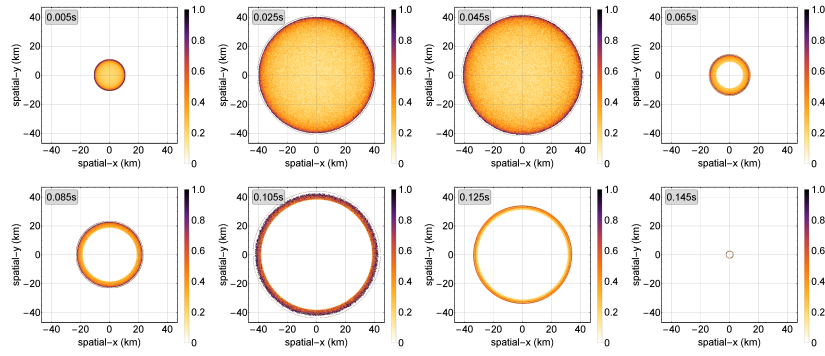


FIG. 2: Evolution of the heavy ions at various snapshots with  $\Gamma \simeq 1.09$ . The figures are viewed in the direction of the ambient magnetic field. The total mass of the initial heavy ions is taken to be 0.02 kg. Other parameters are the same as in Fig. 1. We can see the breathing patterns of the ions in this case.

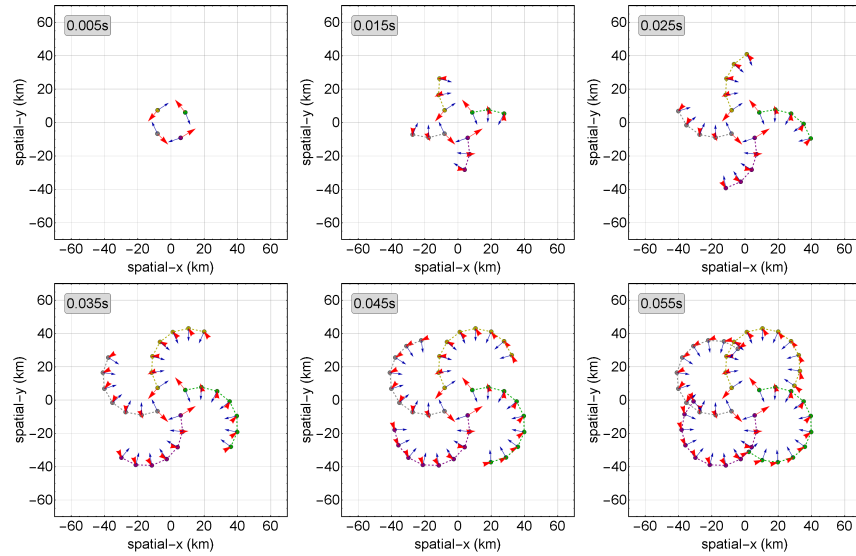


FIG. 3: Motion of the selected debris particles at various snapshots when  $\Gamma \simeq 1.09$ . The parameters are set the same as in Fig. 2. The red and blue arrows in each graph indicate the directions of the electric and magnetic (Lorentz) force received by the particles, respectively. The trajectories of these particles are shown in different colors.

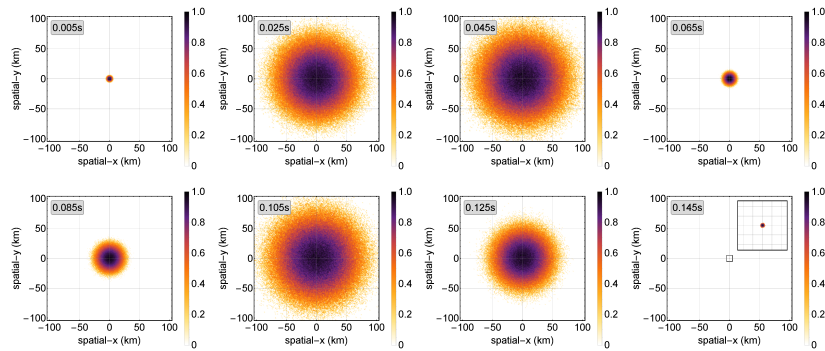


FIG. 4: Evolution of the heavy ions at various snapshots with  $\Gamma \simeq 1.09$ . The figures are viewed in the direction of the ambient magnetic field. The total mass of the initial ions is taken to be 0.02 kg. Initial velocity of the ions is sampled from a Maxwellian distribution with average velocity  $\bar{v}_{i,Fe} = 2 \times 10^6$  m/s. Other parameters are set the same as in Fig. 1.

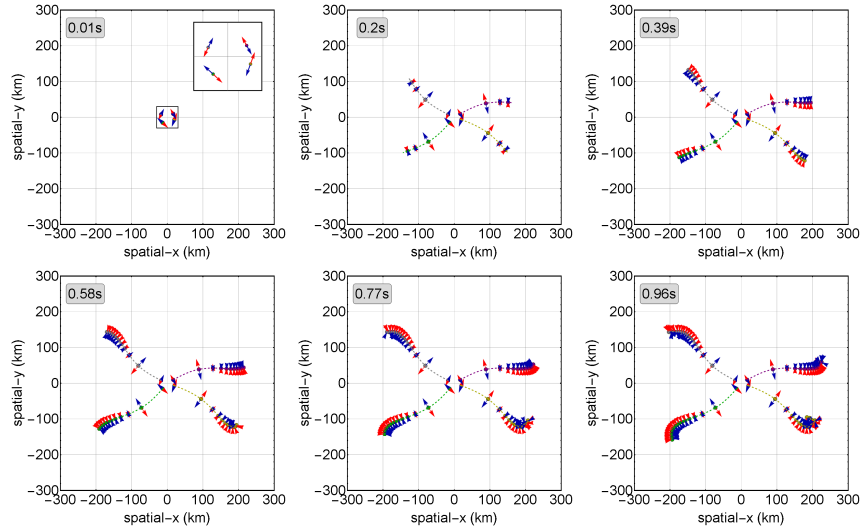


FIG. 5: Motion of the selected ion particles at various snapshots when  $\Gamma \simeq 0.03$ . The parameters are set the same as in Fig. 1. The red and blue arrows in each graph indicate the directions of the electric and magnetic (Lorentz) force received by the particles.

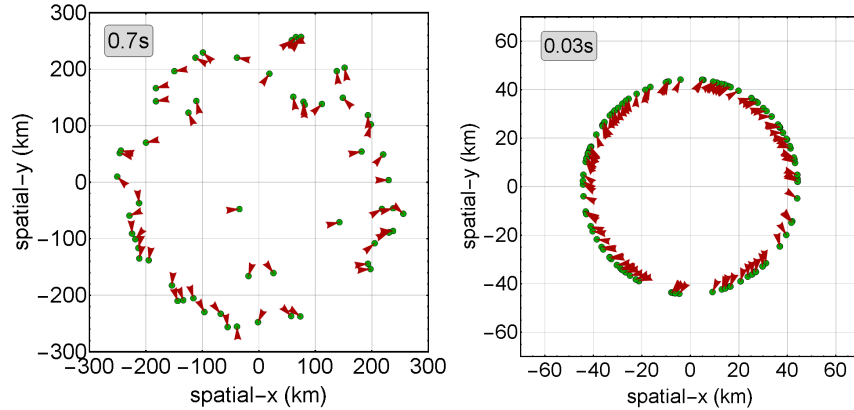


FIG. 6: Directions of the electron drift when  $\Gamma \ll 1$  (left panel) and  $\Gamma \gtrsim 1$  (right panel). Green dots and red arrows represent the selected debris ions and the direction of the associated electron fluid. The arrows are obtained via Eq. (2). The parameters are the same as in Fig. 3 and 5. We see that the electrons can flow in different directions at the rim of the expanding plasma depending on the initial mass of the debris ions.

The second pattern corresponds to the condition where  $\Gamma \simeq 0.03$  as in Fig. 1 and 5. A prominent difference in this condition is a lack of the breathing behavior and a flute mode at the later time (Fig. 1). In Fig. 5 we have selected four ions and plotted their relevant electric and magnetic force. The ions move in an almost straight line. Initially, the Lorentz force is a little larger than the balancing electric force, hence the particles tend to curve slight clockwise. At some later time, the electric force dominates and the ions begin to bend counter-clockwise.

These two different behaviors reveal the complexities of the plasma evolution. A little imbalance of the electric and magnetic force is able to produce two completely different patterns. To see this, we recall that in the hybrid model the electric field is perpendicular to the electron fluid velocity and the magnetic field, i.e.,  $\mathbf{E} = -\mathbf{u}_e \times \mathbf{B}$  (see Eq. (2)). This allows us to analyze the drift of the electrons from the depicted electric force in Fig. 3 and 5. In the breathing pattern where  $\Gamma \gtrsim 1$ , the electrons initially drift outward. When the electron flow reaches the out most rim of the torus, it gradually turns *clockwise*. However, for cases where  $\Gamma \ll 1$ , the electrons drift *counter-clockwise* at the later time. Therefore, the electrons drift in different directions at the rim of the expanding plasma depending on the initial mass of the debris ions (Fig. 6).

Now we analyze the stopping behavior of the two conditions. When  $\Gamma \ll 1$  a strong flute mode will occur, therefore the flute instability should influence the way the heavy ions behave. In Fig. 7 we also plot the trajectories of the four selected ions. The left panel of Fig. 7 shows that the ions are turning counter-clockwise at the later time. This is consistent with the drift direction of the electrons which is also counter-clockwise. However, the right panel demonstrates a rather different behavior — the heavy ions are rotating clockwise in the ambient magnetic field and gradually lose energy.

Finally, we may find some clues of these two phenomena from the building-up equations, i.e., Eq. (4) ~ (6). In Fig. 3 and 5,

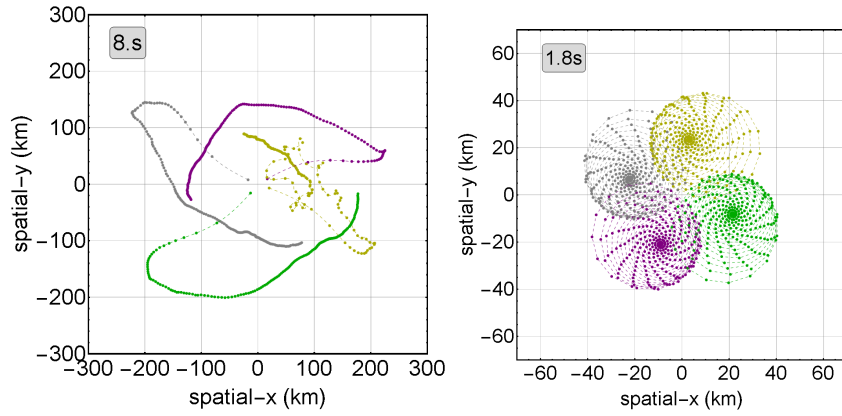


FIG. 7: Trajectories of the heavy ions when  $\Gamma \ll 1$  (left panel) and  $\Gamma \gtrsim 1$  (right panel). The time stamp on the left corner of each graph denotes that only the trajectories before this time is tracked. All parameters are the same as in Fig. 3 and 5.

we can see that the electric force is mainly in the  $\theta$  direction. In Fig. 5, the balancing Lorentz force is also in approximately the  $\theta$  direction initially. When the electric force in the  $\theta$  direction becomes prominent, it curves the trajectories of the ions at the later time (see Fig. 5). The debris ions will then evolve into a flute like pattern. On the contrary, if the Lorentz force is dominant, the debris ions will circulate in the ambient geomagnetic field and evolve toward the breathing like pattern. Therefore, comparing the  $\theta$  component of the electric field will suffice the analysis.

Given that the difference of the phenomenon starts from an imbalance of electric and magnetic force acted upon the heavy ions, we rewrite Eq. (4) in terms of the number densities of the ions  $n_D$  and the background ions  $n_B$ ,

$$\mathbf{E} = -\frac{1}{(n_D + n_B)} \left[ (n_D \mathbf{u}_D + n_B \mathbf{u}_B) \times \mathbf{B} - \frac{1}{\mu_0} (\mathbf{B} \cdot \nabla) \mathbf{B} + \frac{1}{2\mu_0} \nabla B^2 \right], \quad (9)$$

where we have used the identity  $(\nabla \times \mathbf{B} \times \mathbf{B}) = (\mathbf{B} \cdot \nabla) \mathbf{B} - \frac{1}{2} \nabla B^2$ . All ions have charge state +1 with  $\mathbf{J}_D = en_D \mathbf{u}_D$  and  $\mathbf{J}_B = en_B \mathbf{u}_B$ .

From Eq. (16) in the Appendix, we have

$$E_\theta \simeq -\frac{1}{(n_D + n_B)} \left[ -(n_D u_{D,r} + n_B u_{B,r}) B_z - B_z \frac{\partial B_\theta}{\partial z} \right]. \quad (10)$$

For a specific heavy ion with radial velocity  $v_{D,r}$ , the ratio of the electric (in the  $\theta$  direction) to Lorentz force has the following form

$$\frac{E_\theta}{v_{D,r} B_z} = \frac{n_D u_{D,r} + n_B u_{B,r} + \partial B_\theta / \partial z}{(n_D + n_B) v_{D,r}}, \quad (11)$$

where  $v_{D,r} B_z$  gives the Lorentz force in the  $\theta$  direction. For cases where  $\Gamma \ll 1$  as in Fig. 5, the electric force will exceed the Lorentz force at some later time, i.e.,  $E_\theta > v_{D,r} B_z$ . Hence

$$\frac{n_D u_{D,r} + n_B u_{B,r} + \partial B_\theta / \partial z}{(n_D + n_B) v_{D,r}} > 1. \quad (12)$$

Eq. (12) gives a rough criteria for the breathing mode. One sees that the flute like pattern does not purely rely on the number densities, rather it depends on both the number densities and the structure of the magnetic field. However, we emphasize that the criteria in Eq. (12) is directly concluded from the numerical results of the hybrid model. The real plasma evolution should in principle contain the high frequency instabilities and the charge separation effect, etc.

#### IV. CONCLUSION

In the present work, we have studied the phenomenon where a patch of heavy ions expand in a cold background plasma with the existence of an ambient magnetic field. We have simulated two conditions where the initial total mass of the heavy ions is different. The hybrid model results of these two cases demonstrate a distinct collective behavior of the ion's motion. Due to the

imbalance of electric and magnetic force, the heavy ions may involve into a flute like pattern or a breathing like pattern. These patterns reflect a different stopping and collective behavior of the ions. Finally, we also give a rough criteria for the flute like pattern to occur.

Since the contribution of charge separation may not be negligible, a full PIC (Particle-In-Cell) treatment[36] or the direct solving of the coupled relativistic Boltzmann-Maxwell's equations[37] are required. The hybrid simulation model used in this paper assumes that the electrons always appear in such a way that the ions are neutralized, and meanwhile, we have also assumed that displacement current can be neglected in the formulation. These assumptions may not be truly satisfied and may influence the evolution of the plasma system. We will study these factors in detail in our future work.

### Acknowledgments

The authors are thankful for the technical support from Prof. Zhong-Qi Wang in Beijing Institute of Technology. The work is supported by the National Key Research and Development Program of China (NKRDPC) under the grant number:2020YFA0709800. The data that support the findings of this study are openly available in Harvard Dataverse at <https://doi.org/10.7910/DVN/MLZKPS>.

### V. APPENDIX

In cylindrical coordinate the following relations hold

$$\begin{aligned} \mathbf{u} \times \mathbf{B} = & (u_\theta B_z - u_z B_\theta) \hat{r} \\ & + (u_z B_r - u_r B_z) \hat{\theta} \\ & + (u_r B_\theta - u_\theta B_r) \hat{z}, \end{aligned} \quad (13)$$

$$\frac{1}{2\mu_0} \nabla \mathbf{B}^2 = \frac{1}{2\mu_0} \left( \frac{\partial \mathbf{B}^2}{\partial r} \hat{r} + \frac{1}{r} \frac{\partial \mathbf{B}^2}{\partial \theta} \hat{\theta} + \frac{\partial \mathbf{B}^2}{\partial z} \hat{z} \right), \quad (14)$$

and

$$\begin{aligned} -\frac{1}{\mu_0} (\mathbf{B} \cdot \nabla) \mathbf{B} = & -\frac{1}{\mu_0} \left[ \left( B_r \frac{\partial B_r}{\partial r} + \frac{B_\theta}{r} \frac{\partial B_r}{\partial \theta} + B_z \frac{\partial B_r}{\partial z} - \frac{B_\theta^2}{r} \right) \hat{r} \right. \\ & + \left( B_r \frac{\partial B_\theta}{\partial r} + \frac{B_\theta}{r} \frac{\partial B_\theta}{\partial \theta} + B_z \frac{\partial B_\theta}{\partial z} + \frac{B_\theta B_r}{r} \right) \hat{\theta} \\ & \left. + \left( B_r \frac{\partial B_z}{\partial r} + \frac{B_\theta}{r} \frac{\partial B_z}{\partial \theta} + B_z \frac{\partial B_z}{\partial z} \right) \hat{z} \right], \end{aligned} \quad (15)$$

where  $\mathbf{u} \equiv n_D \mathbf{u}_D + n_B \mathbf{u}_B$ . If we restrict our analysis in the spatial  $x-y$  plane, the  $\hat{r}$  and  $\hat{\theta}$  components of the electric field  $E_r$  and  $E_\theta$  will suffice. In the expansion of the debris ions,  $u_r$  should be larger than  $u_z$ , hence  $u_z B_r \ll u_r B_z$  in Eq. (13).

From Fig. 3 and 5, we can see that the electric force is nearly symmetrical in the  $\theta$  direction. This allows us to drop the terms  $\frac{1}{r} \frac{\partial \mathbf{B}^2}{\partial \theta} \hat{\theta}$  and  $\frac{B_\theta}{r} \frac{\partial B_\theta}{\partial \theta}$ . Meanwhile, the contribution of the term  $B_z \frac{\partial B_\theta}{\partial z}$  is larger than terms  $B_r \frac{\partial B_\theta}{\partial r}$  and  $\frac{B_\theta B_r}{r}$  (see the numerical comparison in Fig. 8). Therefore, we can express the  $\hat{\theta}$  component of the electric field  $E_\theta$  in terms of  $B_z$ ,

$$E_\theta \simeq -\frac{1}{(n_D + n_B)} \left[ -(n_D u_{D,r} + n_B u_{B,r}) B_z - B_z \frac{\partial B_\theta}{\partial z} \right]. \quad (16)$$

One may find that Eq. (16) is different from the one expressed in [1], where

$$E_\theta \simeq -\frac{1}{(n_D + n_B)} [-(n_D u_{D,r} + n_B u_{B,r}) B_z]. \quad (17)$$

This is because in our analysis, the deviation of two different phenomena takes place at a much later time than in [1]. Thus, the contribution of the term  $\nabla \times \mathbf{B} \times \mathbf{B}$  cannot be neglected.

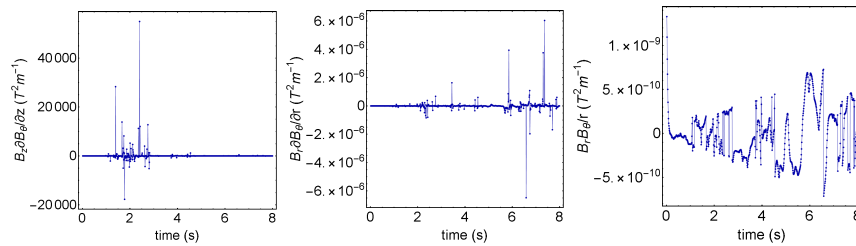


FIG. 8: Comparison of the terms  $B_z \frac{\partial B_\theta}{\partial z}$ ,  $B_r \frac{\partial B_\theta}{\partial r}$  and  $\frac{B_\theta B_r}{r}$ . The parameters are the same as in Fig. 1. The data is extracted from one of the four selected particles in Fig. 5. We can see that the contribution of the term  $B_z \frac{\partial B_\theta}{\partial z}$  is significantly larger than that of other terms.

- [2] S. H. Brecht, D. W. Hewett, and D. J. Larson, *Geophysical Research Letters* **36** (2009).
- [3] D. Winske, J. D. Huba, C. Niemann, and A. Le, *Frontiers in Astronomy and Space Sciences* **5** (2019).
- [4] Q. Pognan, C. Garraffo, O. Cohen, and J. J. Drake, *The Astrophysical Journal* **856** (2018).
- [5] M. L. Goldstein, J. P. Eastwood, R. A. Treumann, E. A. Lucek, J. Pickett, and P. Décréau, *Space Science Reviews* **118** (2005).
- [6] S. J. Hofmeister, A. M. Veronig, S. Poedts, E. Samara, and J. Magdalenic, *The Astrophysical Journal Letters* **897** (2020).
- [7] T. K. Kim, R. W. Ebert, P. W. Valek, F. Allegrini, D. J. McComas, F. Bagenal, J. E. P. Connerney, G. Livadiotis, M. F. Thomsen, R. J. Wilson, et al., *Journal of Geophysical Research: Space Physics* **125** (2020).
- [8] Y. Yamazaki, Y. Miyoshi, C. Xiong, C. Stolle, G. Soares, and A. Yoshikawa, *Journal of Geophysical Research: Space Physics* **125** (2020).
- [9] A. Bultel, J. Annaloro, and V. Morel, *Journal of Physics: Conference Series* **399** (2012).
- [10] L. Campbell and M. J. Brunger, *PLASMA SOURCES SCIENCE AND TECHNOLOGY* **22** (2013).
- [11] J. Zinn, H. Hoerlin, and A. G. Petscheck, McCormac (ed.) *Radiation Trapped*. (1963).
- [12] Y. P. Raizer and S. T. Surzhikov, *AIAA Journal* **33** (1995).
- [13] W. J. McDoniel, D. B. Goldstein, P. L. Varghese, and L. M. Trafton, *Physics of Fluids* **31** (2019).
- [14] G. Sinibaldi, A. Occhicone, F. A. Pereira, D. Caprini, L. Marino, F. Michelotti, and C. M. Casciola, *Physics of Fluids* **31** (2019).
- [15] M. Ishaq and H. Xu, *Physics of Fluids* **31** (2019).
- [16] R. A. Treumann, *Astron Astrophys Rev* (2009).
- [17] D. D. Ryutov, *Plasma Physics and Controlled Fusion* **61** (2018).
- [18] H. Akimune, I. Ikeda, T. Hirata, and F. Okamoto, *Journal of the Physical Society of Japan* **50** (1981).
- [19] V. Kopecky, *NUCLEAR FUSION* (1968).
- [20] S. P. Garyand and D. Winske, *JOURNAL OF GEOPHYSICAL RESEARCH* (1990).
- [21] D. S. Harned, *Journal of Computational Physics* (1982).
- [22] D. W. Hewett, *Journal of Computational Physics* (1980).
- [23] V. A. Thomas and S. H. Brecht, *Physics of Fluids* **29** (1986).
- [24] V. A. Thomas and Stephen, *Journal of Geophysical Research* **92** (1987).
- [25] D. Winske and S. P. Gary, *Journal of Geophysical Research* **112** (2007).
- [26] A. V. Artemyev, V. Angelopoulos, I. Y. Vasko, A. Runov, L. A. Avanov, B. L. Giles, C. T. Russell, and R. J. Strangeway, *Geophysical Research Letters* **43** (2019).
- [27] G. G. Howes, *PHYSICS OF PLASMAS* **25** (2018).
- [28] I. F. Shaikhislamova, Y. P. Zakharova, V. G. Posukha, A. V. Melekhova, E. L. Boyarintseva, A. G. Ponomarenkoa, and V. A. Terekhinb, *Plasma Physics Reports* **41** (2015).
- [29] D. B. Schaeffer, W. Fox, D. Haberberger, G. Fiksel, A. Bhattacharjee, D. H. Barnak, S. X. Hu, and K. Germaschewski, *PHYSICAL REVIEW LETTERS* **119** (2017).
- [30] G. Ganguli, C. Crabtree, M. Mithaiwala, L. Rudakov, and W. Scales, *Physics of Plasmas* **22** (2015).
- [31] A. Valenzuela, G. Haerendel, H. Foppl, F. Melzner, H. Neuss, E. Rieger, J. Stocker, O. Nauer, H. Hofner, and J. Loidl, *Nature* **320** (1986).
- [32] P. V. Heuer, M. S. Weidl, R. S. Dorst, D. B. Schaeffer, A. S. Bondarenko, S. K. P. Tripathi, B. V. Compennolle, S. Vincena, C. G. Constantin, C. Niemann, et al., *Physics of Plasmas* **25** (2018).
- [33] M. R. Gibbons and D. W. Hewett, *Journal of Computational Physics* (1995).
- [34] A. Marcowith, A. Bre, A. Bykov, M. E. Dieckman, L. O. Drury, B. Lembège, M. Lemoine, G. Morlino, G. Murphy, G. Pelletier, et al., *Reports on Progress in Physics* (2016).
- [35] H. Yoshihara, *Physics of Fluids* **4** (1961).
- [36] K. J. Bowers, B. J. Albright, L. Yin, B. Bergen, and T. J. T. Kwan, *Phys. Plasmas* **15** (2008).
- [37] J.-J. Zhang, H.-Z. Wu, S. Pu, G.-Y. Qin, and Q. Wang, *Physical Review D* **102** (2020).